AGU PUBLICATIONS

Geochemistry, Geophysics, Geosystems

RESEARCH ARTICLE
10.1002/2013GC005067

Key Points:
- Report a new data set of landslides triggered by the 2008 Wenchuan earthquake
- Develop a quantitative model to estimate earthquake volume balance
- Evaluate how earthquakes of varying magnitude contribute to coseismic mountain building

Supporting Information:
- Supporting information readme
- Figures S1–S7
- Tables S1–S4

Correspondence to:
Gen Li,
genli@usc.edu

Citation:
Li, G., A. J. West, A. L. Densmore, Z. Jin, R. N. Parker, and R. G. Hilton (2014), Seismic mountain building: Landslides associated with the 2008 Wenchuan earthquake in the context of a generalized model for earthquake volume balance, *Geochem. Geophys. Geosyst.*, *15*, doi:10.1002/2013GC005067.

Received 30 SEP 2013
Accepted 14 JAN 2014
Accepted article online 20 JAN 2014

Seismic mountain building: Landslides associated with the 2008 Wenchuan earthquake in the context of a generalized model for earthquake volume balance

Gen Li[1], A. Joshua West[1], Alexander L. Densmore[2], Zhangdong Jin[3], Robert N. Parker[4], and Robert G. Hilton[2]

[1]Department of Earth Sciences, University of Southern California, Los Angeles, California 90089, USA, [2]Department of Geography, Institute of Hazard, Risk and Resilience, Durham University, Durham, UK, [3]State Key Laboratory of Loess and Quaternary Geology, Institute of Earth Environment, Chinese Academy of Sciences, Xi'an, China, [4]School of Earth and Ocean Sciences, Cardiff University, Cardiff, UK

Abstract Here we assess earthquake volume balance and the growth of mountains in the context of a new landslide inventory for the M_w 7.9 Wenchuan earthquake in central China. Coseismic landslides were mapped from high-resolution remote imagery using an automated algorithm and manual delineation, which allow us to distinguish clustered landslides that can bias landslide volume calculations. Employing a power-law landslide area-volume relation, we find that the volume of landslide-associated mass wasting ($\sim 2.8 + 0.9/-0.7$ km^3) is lower than previously estimated ($\sim$5.7–15.2 km^3) and comparable to the volume of rock uplift ($\sim 2.6 \pm 1.2$ km^3) during the Wenchuan earthquake. If fluvial evacuation removes landslide debris within the earthquake cycle, then the volume addition from coseismic uplift will be effectively offset by landslide erosion. If all earthquakes in the region followed this volume budget pattern, the efficient counteraction of coseismic rock uplift raises a fundamental question about how earthquakes build mountainous topography. To provide a framework for addressing this question, we explore a group of scaling relations to assess earthquake volume balance. We predict coseismic uplift volumes for thrust-fault earthquakes based on geophysical models for coseismic surface deformation and relations between fault rupture parameters and moment magnitude, M_w. By coupling this scaling relation with landslide volume-M_w scaling, we obtain an earthquake volume balance relation in terms of moment magnitude M_w, which is consistent with the revised Wenchuan landslide volumes and observations from the 1999 Chi-Chi earthquake in Taiwan. Incorporating the Gutenburg-Richter frequency-M_w relation, we use this volume balance to derive an analytical expression for crustal thickening from coseismic deformation based on an index of seismic intensity over a defined area. This model yields reasonable rates of crustal thickening from coseismic deformation (e.g., $\sim$0.1–0.5 km Ma^{-1} in tectonically active convergent settings), and implies that moderate magnitude earthquakes ($M_w \approx$ 6–7) are likely responsible for most of the coseismic contribution to rock uplift because of their smaller landslide-associated volume reduction. Our first-order model does not consider a range of factors (e.g., lithology, climate conditions, epicentral depth, and tectonic setting), nor does it account for viscoelastic effects or isostatic responses to erosion, and there are important large uncertainties on the scaling relationships used to quantify coseismic deformation. Nevertheless, our study provides a conceptual framework and invites more rigorous modeling of seismic mountain building.

1. Introduction

Earthquakes are thought to contribute substantially to tectonic uplift and orogenic growth [*Avouac*, 2007]. However, earthquakes can also result in widespread landsliding in mountain belts, leading to enhanced erosion and thus working to reduce surface topography [*Keefer*, 1994; *Dadson et al.*, 2004; *Guzzetti et al.*, 2009; *Korup et al.*, 2010; *Hovius et al.*, 2011; *Egholm et al.*, 2013]. Notably, it has been observed that large, shallow earthquakes trigger mass wasting that can effectively offset or even outweigh the coseismic addition of rock mass or volume to an orogen [*Hovius et al.*, 2011; *Parker et al.*, 2011]. Quantifying this earthquake volume balance, or the net result of coseismic mass wasting and coseismic crustal growth, is critical for understanding crustal mass budgets, landscape building, and the role of earthquakes in mountain belt evolution.

Previous studies have estimated the volume balance for individual earthquakes through mapping landslides from remote imagery, gauging riverine sediment load, and measuring surface displacements within the

zones of concentrated slip and moment release [e.g., *Hovius et al*., 2011; *Parker et al*., 2011], but less attention has been paid to develop a general volume balance relation for earthquakes. The general volume balance equation for a single earthquake depends on the deficit term from landsliding and fluvial evacuation and the surplus term from coseismic fault slip and rock deformation. Additional volume loss over repeated earthquake cycles can result from fluvial and diffusive hillslope erosion and landslides not associated with earthquake triggering, and additional volume gain can result from aseismic and interseismic slip, and from viscoelastic, isostatic, or dynamic effects. However, here we focus specifically on the coseismic volume balance, which has heretofore been difficult to isolate from the interseismic processes. An empirical correlation between the total landslide volume triggered by an earthquake and the earthquake's moment magnitude M_w has been reported [*Keefer*, 1994], and this provides a generalizable constraint on the deficit of the volume balance. Increasing landslide area and volume with earthquake magnitude is related to the triggering of landslides by ground motion, and is modulated by topographic effects and seismic wave attenuation, which together have been shown to control the rate and distribution of coseismic landslides [*Meunier et al*., 2007].

For the volume surplus term, two-dimensional dip-slip dislocation models simulate coseismic crustal deformation, and these are well validated by field observations [*Okada*, 1985, 1992; *Cohen*, 1996]. Together with statistical correlations between fault rupture parameters and earthquake magnitudes [*Wells and Coppersmith*, 1994], these models make it possible to relate earthquake magnitude to the volume of material added to the upper crust. With the deficit and surplus terms thus constrained, an analytical volume balance equation for earthquakes with specified magnitudes can be derived. By introducing the Gutenburg-Richter frequency-magnitude relation and a regional seismic-intensity factor, we can further derive an analytical expression for coseismic crustal thickening rates in terms of the frequency of occurrence of earthquakes. These thickening rates represent the cumulative effects from coseismic tectonic volume addition and landslide erosion for all earthquakes in a given region.

In this study, we combine new landslide data for the Wenchuan earthquake and the derivation of this general volume balance relation to investigate the problem of earthquake volume budgets. The M_w 7.9 Wenchuan earthquake occurred in an area of steep mountainous topography and caused widespread coseismic landsliding [*Dai et al*., 2011; *Parker et al*., 2011]. It thus provides an ideal case study for evaluating earthquake volume balance. We first report a new coseismic and immediate postseismic landslide data set for the Wenchuan earthquake, developed through mapping using high-resolution remote imagery covering the rupture zones. We calculate the total landslide volume using a power-law landslide area-volume relation [*Guzzetti et al*., 2009; *Larsen et al*., 2010], and compare the landslide volume to the surface uplift measured from synthetic aperture radar (SAR) [*de Michele et al*., 2010; *Parker et al*., 2011]. Our result from Wenchuan is then used, together with data from the 1999 Chi-Chi earthquake in Taiwan, to test our general model for describing earthquake volume balance. Although the very large uncertainties in the parameterizations used in our analysis make it difficult to confidently discern positive versus negative volume balance, we view the conceptual framework presented here as providing a potentially valuable foundation for future work that may reduce these uncertainties.

2. Setting

The M_w 7.9 Wenchuan earthquake occurred on 12 May 2008 in the Longmen Shan mountain range, Sichuan Province, central China. The regional lithology is characterized by mixed assemblages of Proterozoic basement rocks, a Paleozoic passive margin sequence, a Mesozoic foreland basin succession, and limited exposures of Cenozoic sediment [*Burchfiel et al*., 1995]. The faults within the region are mainly dextral-thrust oblique-slip faults, which initiated in the Late Triassic and have been active through the Cenozoic [*Densmore et al*., 2007]. Based on modern geodetic observations and paleoseismology, the recurrence time of large earthquakes within the Longmen Shan range is estimated to be ~2000–4000 years [*Ran et al*., 2010; *Shen et al*., 2009]. Geophysical observations show that fault displacement varied greatly along the surface rupture, with two areas, Yingxiu and Beichuan, suffering the largest slip and moment release (Figure 1) [*Liu-Zeng et al*., 2009; *Shen et al*., 2009].

3. Methods

We first used unsupervised classification based on spectral intensities [e.g., *Borghuis et al*., 2007; *Parker et al*., 2011; *West et al*., 2011] to identify and extract landslide areas from satellite imagery. We used high-

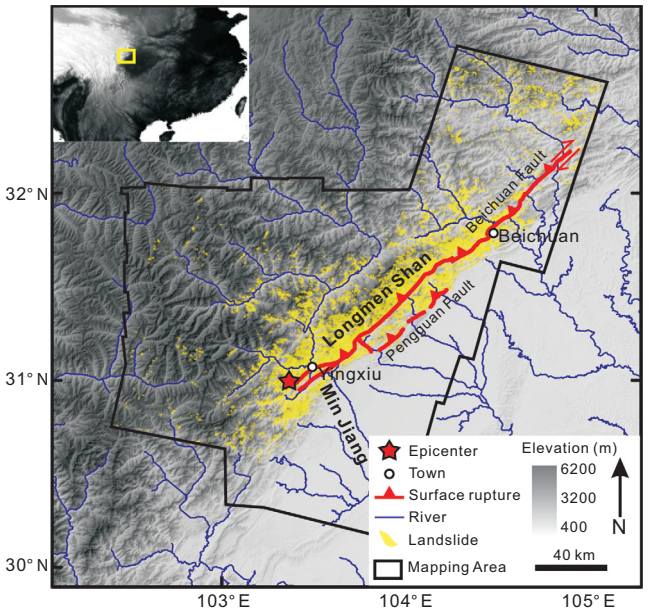

Figure 1. Regional topography of the Longmen Shan region, China, and location (red star) of the M_w 7.9 Wenchuan earthquake, China, with surface rupture traces (red lines) [*Liu-Zeng et al*., 2009; *Xu et al*., 2009] and mapped coseismic landslides (yellow polygons). The black-outlined polygon shows the landslide mapping area.

resolution satellite imagery (SPOT, Digital Globe WorldView and QuickBird images) taken within 1 month after the earthquake. Our landslide mapping was conducted over 38,270 km^2 in the Longmen Shan, covering over 90% of the surface rupture area and the zones of most concentrated landslide density. Using manual screening, we then removed nonlandslide objects including roads, buildings, and terraces based on visual contrast and spatial characteristics of landslide locations. Large clusters of amalgamated landslides were segmented into their constituent parts and each individual landslide was delineated manually (see supporting information). The mapped landslides were then compared to images from before the earthquake to eliminate preexisting landslides.

4. Results

Within the Longmen Shan region, we mapped a total of 57,150 landslides, with a total area of ~396 km^2, which is much smaller than the previous estimate (~566 km^2) by *Parker et al*. [2011]. The probability density of all landslides is well described by a three-parameter inverse-gamma distribution (see supporting information), as observed for many other landslide inventories [*Malamud et al*., 2004].

The conversion from area to volume for each individual landslide is implemented via a power-law scaling relationship [*Hovius et al*., 2011; *Larsen et al*., 2010]:

$$V_L = \sum_{i=1}^{n} \alpha A_{Li}^{\gamma} \quad (1)$$

where V_L is the total volume of landslide material, A_{Li} is the area of the ith landslide, n is the number of mapped landslides, and α and γ are empirical scaling parameters. Based on this relationship, the total landslide volume for the Wenchuan landslides is calculated as ~2.8 + 0.9/−0.7 km^3 by using published scaling parameters [*Guzzetti et al*., 2009; *Larsen et al*., 2010] including those obtained from field measurements of 41 coseismic landslides in the Longmen Shan [*Parker et al*., 2011] (Table 1). The value and uncertainty of the total landslide volume are determined by Monte Carlo simulation taking into account combinations of the two scaling parameters α and γ. For each group of parameters, volume calculations (i.e., equation (1)) on the Wenchuan landslide inventory were repeated 50,000 times with random sampling of normally distributed scaling parameters α and γ, and the total landslide volume value is reported based on the median of the Monte Carlo distribution with lower and upper bounds defined by the 16th and 84th percentiles of the distribution, respectively (Tables 1 and S3). To account for variations among different combinations of parameters, a combined total landslide volume value and relevant uncertainties (2.8 + 0.9/−0.7 km^3) are then calculated by applying this sampling algorithm to all combinations of scaling parameters (Table 1, Table S3 and details in supporting information). Sensitivity analysis indicates that the most significant source of uncertainty in the final calculation of total landslide volume is from the uncertainty in the

Table 1. Landslide Area-Volume Scaling Relationships Applicable to the Wenchuan Region [*Parker et al*., 2011] and Estimated Total Landslide Volumes[a]

Parameter	$\log_{10}\alpha$	γ	Volume (km^3)	Reference
L1 (global landslides)	-0.836 ± 0.015	1.332 ± 0.005	$1.80 + 0.12/-0.11$	*Larsen et al*. [2010]
L2 (global bedrock landslides)	-0.73 ± 0.06	1.35 ± 0.01	$2.81 + 0.39/-0.35$	*Larsen et al*. [2010]
L3 (mixed Himalayan landslides	-0.59 ± 0.03	1.36 ± 0.01	$4.34 + 0.55/-0.49$	*Larsen et al*. [2010]
G (global landslides)	-1.131	1.45 ± 0.009	$3.49 + 0.39/-0.35$	*Guzzetti et al*. [2009]
P1 (Longmen Shan landslides)	-0.974 ± 0.366	1.388 ± 0.087	$2.50 + 6.72/-1.81$	*Parker et al*. [2011]
P2 (Longmen Shan landslides)	-0.995 ± 0.366	1.392 ± 0.087	$2.48 + 6.62/-1.79$	This study
Combined (see supporting information)			$2.83 + 0.86/-0.65$	

[a]For the Longmen Shan landslide parameters, P1 refers to parameters obtained from an ordinary regression on the Longmen Shan landslide field measurement data set [*Parker et al*., 2011]; P2 refers to parameters from a robust regression on the same data set. For each group of scaling parameters, volumes and errors are obtained via a Monte Carlo sampling strategy. For the reported total landslide volume in the text, calculations for each individual landslide are repeated 50,000 times using all the combinations of the cited scaling parameters, and mean values for each landslide are summed to give the total volume. All values are reported based on the median of the Monte Carlo distribution with lower and upper bounds defined by the 16th and 84th percentiles of the distribution (i.e., ranges of $\pm$1SD in a standard normal distribution), respectively.

parameter γ (see Figure S6 and Table S4 in supporting information). The estimated landslide volume range (2.1–3.7 km^3) is consistent with the volume range (1.5–3.6 km^3) reported in a recent study [*Ren et al*., 2014], which determined well-constrained volumes within smaller spatial windows in the Longmen Shan and extrapolated these to the total area of coseismic landslides assuming a lognormal distribution.

The global correlation between the total volume of landslides triggered by an earthquake V_L and the earthquake moment magnitude M_w [*Keefer et al*., 1994; *Malamud et al*., 2004] provides context for interpreting the estimated volumes from the Wenchuan earthquake:

$$\log V_L = 1.42M_w - 11.26(\pm 0.52) \quad (2)$$

For $M_w = 7.9$, this global scaling relationship gives a total landslide volume V_L of $0.9 + 2.1/-0.6$ km^3, or a range of 0.3–3.0 km^3. This compares to our estimation from mapping of $V_L = \sim 2.8 + 0.9/-0.7$ (2.1–3.7) km^3. Although the mean volume derived from our mapping is higher than the mean inferred from the global scaling relationship, the ranges clearly overlap considering the uncertainties. This type of comparison could be improved by further efforts to reduce uncertainties both in the global relationships and in the area-volume parameters used to determine landslide volume from individual earthquakes such as Wenchaun.

5. Discussion

5.1. The Wenchuan Earthquake Volume Balance

The coseismic volume addition to the Longmen Shan region resulting from slip during the Wenchuan earthquake is $\sim 2.6 \pm 1.2$ km^3 based on synthetic aperture radar (SAR) data [*de Michele et al*., 2010; *Parker et al*., 2011]. This range is close to our estimated total landslide volume ($2.8 + 0.9/-0.7$ km^3). Although the large uncertainties on both values limit our ability to confidently distinguish between positive and negative net volume balances, the first-order similarity between the volume growth and potential reduction due to landslides implies that, for the Wenchuan earthquake at least, seismically triggered landslide erosion can significantly offset coseismic tectonic rock uplift if all of the landsliding material can be evacuated by rivers before the next comparable earthquake. Incomplete fluvial evacuation of landslide material is unlikely to affect the long-term volume budget (e.g., over the time scale of repeated earthquake cycles), because it would require long-term accumulation of very significant amounts of landslide debris, at odds with the thin alluvial cover on hillslopes and lack of thick pre-2008 sediment stores in the Longmen Shan [*Ouimet et al*., 2009; *Parker et al*., 2011]. Thus, from a volume balance perspective, the contribution from coseismic deformation during the Wenchuan earthquake to the long term, regionally averaged topographic evolution of the Longmen Shan range is considerably reduced by coseismic landslides, and may be close to insignificant.

Our calculated landslide volume ($2.8 + 0.9/-0.7$ km^3) is lower than the previously reported volume range of 5–15 km^3 [*Parker et al*., 2011]. This previous work used only an automated algorithm to extract landslides. We added rigorous manual screening after noticing that the automated routine did not separate amalgamated clusters of landslides into their component parts. Segregation of amalgamated clusters has a large

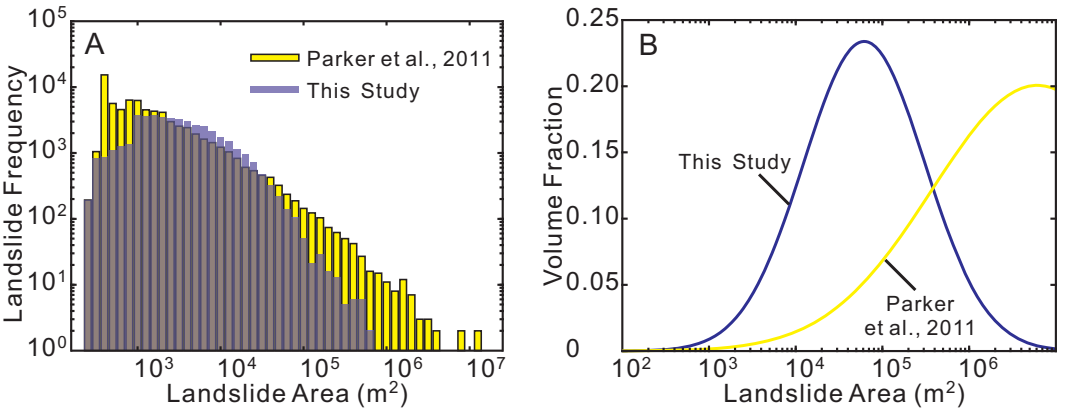

Figure 2. Comparison between the landslide inventories from this study and *Parker et al.* [2011]. (a) Landslide area distributions in logarithmic space. The landslide data set in *Parker et al.* [2011] contains substantially more large landslides. This long tail is due to clustered landslides and explains the larger volume calculated by *Parker et al.* [2011] compared to this study (see supporting information). (b) Contributions to total calculated volumes from different landslide groups. Compared to *Parker et al.* [2011], landslides of moderate area contribute most to the total volume in this study.

potential effect on estimated landslide volumes because of the nonlinear relationship between landslide area and volume [*Guzzetti et al.*, 2009; *Larsen et al.*, 2010]. The ratio of the volumes from our study compared to *Parker et al.* [2011] falls on a predetermined curve controlled by the splitting of clumped landslides (see supporting information); any difference between the studies in screening for nonlandslide areas has minimal effect. The significant differences in calculated volumes demonstrate that large landslide areas not divided into their constituent parts (i.e., the long tail in Figure 2a) can strongly bias estimates of landslide volumes (consider the contributions of different-sized landslides to the total landslide volume, as shown Figure 2b).

While the differences between the revised landslide volume estimate presented here and the previously reported volume from *Parker et al.* [2011] highlight the importance of differentiating individual landslides from clustered landslide during automated mapping at large scales, it is worth noting that both results lead to the same conclusion that earthquake-triggered mass wasting may effectively offset coseismic volume addition. Although accurate net coseismic volume difference cannot be confidently determined within the uncertainties in the data and the methodology used here, the similarity of the volume estimates is a key observation that requires further consideration.

If other earthquakes follow the same pattern, the volume budget for Wenchuan poses important questions about coseismic mountain building [*Parker et al.*, 2011]. One explanation for the efficient counteraction of coseismic volume addition in the Wenchuan case may be that erosion and uplift are indeed balanced in the present-day Longmen Shan [*Godard et al.*, 2009]. Another is that isostatic compensation for removed landslide material counteracts mass wasting and facilitates rock uplift [*Molnar*, 2012]. Simple calculation of the flexural-isostatic response of the Longmen Shan range, however, indicates that erosionally induced rock uplift could only replace ~30% of the mass lost from landslides [*Densmore et al.*, 2012]. Here we explore another possibility: that orogenic growth is controlled by the imbalance between volume accumulation in small earthquakes which trigger low volumes of landslides, and volume destruction from large earthquakes which trigger large landslide volumes [*Parker et al.*, 2011]. In that scenario, the coseismic orogenic volume balance should depend significantly on earthquake magnitudes.

5.2. Volume Balance for Earthquake Events With Specified Moment Magnitudes

We examine the relationship between earthquake volume balance and earthquake magnitude using a first-order quantitative model informed by empirical scaling relationships. We relate the volume budget of an individual earthquake event to the earthquake's moment magnitude by considering (1) the total landslide volume-magnitude relation for a given event [*Keefer*, 1994], (2) the analytical deformation field for an earthquake event from a two-dimensional dip-slip dislocation model, and (3) scaling relations between fault rupture parameters (e.g., rupture area, surface displacement, and rupture length) and earthquake magnitude [*Wells and Coppersmith*, 1994].

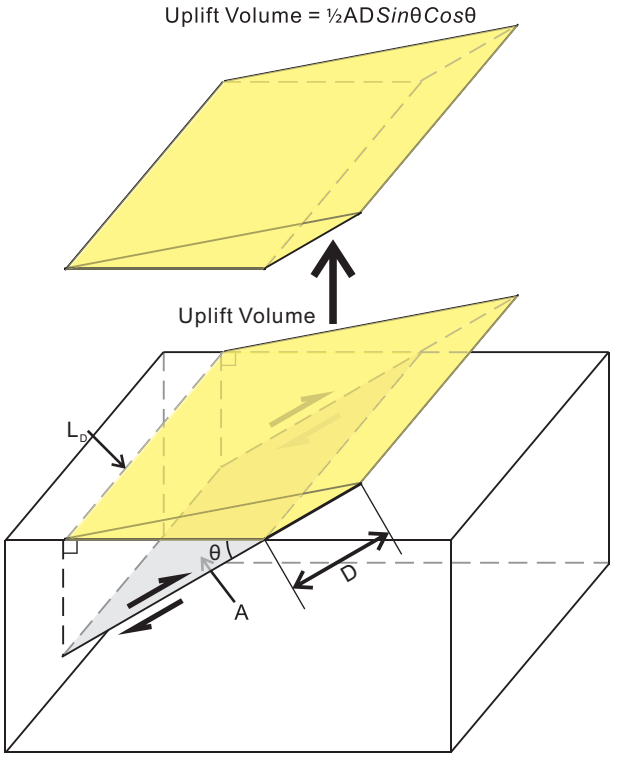

Figure 3. A 3-D geometrical model showing the uplift volume due to slip on a thrust fault in terms of rupture area *A*, surface displacement *D*, and dip angle θ. The volume added by fault slip in this geometrical model is effectively equal to the calculated volume from the analytical deformation field for the two-dimensional dip-slip dislocation model (see supporting information). The dashed line L_D represents the position of zero surface strain [*Fu et al*., 2011].

Based on the analytical deformation field for a two-dimensional dip-slip dislocation model in a homogeneous, elastic half-space [*Okada*, 1985, 1992], we calculate the uplift volume caused by the surface deformation of a thrust-fault earthquake by integrating the vertical displacement over the uplifted range (see supporting information). The integrated result can be expressed geometrically as an extruded volume (the yellow colored region in Figure 3). The uplifted volume V_U is expressed as a function of fault rupture area *A*, surface displacement *D*, and dip angle θ (see supporting information):

$$V_U = \frac{1}{2} AD \sin\theta \cos\theta \tag{3}$$

To minimize the effects from dip angle θ and to average the uplifted volume over the dip angle, we define a dip angle averaging term Θ as:

$$\Theta = \frac{\int_{\theta_{\min}}^{\theta_{\max}} \frac{1}{2} \sin\theta \cos\theta \, d\theta}{\int_{\theta_{\min}}^{\theta_{\max}} d\theta} \tag{4}$$

where Θ is used to normalize the uplift volume as a function of dip angle θ over a range of dip angles. Integration over the dip angle range ($\theta_{\min} \le \theta \le \theta_{\max}$) gives the dip angle-averaged uplifted volume:

$$\bar{V}_U = AD\Theta \tag{5}$$

The well-constrained fault geometry of the Wenchuan earthquake [*Xu et al*., 2009] can be used to examine this uplift volume model in comparison with the results from SAR-based geodetic observations [*de Michele et al*., 2010]. With the fault geometric parameters (focal depth ~14–18 km, subsurface-surface dip angle ~40° to ~90°, and rupture length ~240 km) from *Xu et al*. [2009] and our integration method (equations (3)–(5)), we estimate the 2008 Wenchuan earthquake rock uplift volume as 3.5 ± 0.9 km^3, which overlaps within uncertainty with the SAR-based rock uplift volume of 2.6 ± 1.2 km^3. This suggests that our simplified, two-dimensional dip-slip dislocation model provides a reasonable first-order constraint on uplift volumes.

To generalize this uplift volume model, we adopted empirical relationships between fault rupture area, surface displacement, and moment magnitude M_w from *Wells and Coppersmith* [1994], which were reported as:

$$\log A = a_A + b_A M_w \tag{6}$$

$$\log D = a_D + b_D M_w \tag{7}$$

where a_A, b_A, a_D, and b_D are the empirical constants. By combining these with equation (5), we obtain an expression relating the dip angle-averaged uplifted volume and M_w:

$$\log \bar{V}_U = (a_A + a_D) + (b_A + b_D) M_w + \log\Theta \tag{8}$$

Table 2. Model Parameters

Variable	Description	Equation Introduced	Reference
A_L	area of landslide	1	
V_L	volume of landslide	1	
α	coefficient in landslide area-volume relation	1	*Larsen et al.*, 2010; *Guzzetti et al.*, 2009; *Parker et al.*, 2011
γ	coefficient in landslide area-volume relation	1	*Larsen et al.*, 2010; *Guzzetti et al.*, 2009; *Parker et al.*, 2011
M_w	earthquake moment magnitude	2	
V_U	coseismic uplift volume	3	
A	rupture area	3	
D	rupture surface displacement	3	
θ	dip angle of thrust faults	3	
$\theta_{\max}$ θ_{min}	maximum and minimum dig angles of mountain building-associated thrust faults	4	
Θ	Theta function for averaging the dip angle term in the uplift volume over a given range	4	
$\bar{V}_U$	dip angle-averaged uplift volume	5	
a_A	scaling factor in rupture area-magnitude relation, -3.99±0.36 (±1 S.D.) for reverse faults	6	*Wells and Coppersmith*, 1994
b_A	scaling factor in rupture area-magnitude relation,0.98±0.06 (±1 S.D.) for reverse faults	6	*Wells and Coppersmith*, 1994
a_D	scaling factor in surface displacement-magnitude relation, -0.74±1.40 (±1 S.D.) for reverse faults	7	*Wells and Coppersmith*, 1994
b_D	scaling factor in surface displacement-magnitude relation, 0.08±0.21 (±1 S.D.) for reverse faults	7	*Wells and Coppersmith*, 1994
a_L	scaling factor in landslide volume-magnitude relation, -11.26±0.52 (±1 S.D.)	13	*Keefer*, 1994; *Malamud et al.*, 2004
b_L	scaling factor in landslide volume-magnitude relation,1.42	13	*Keefer*, 1994; *Malamud et al.*, 2004
$\dot{a}_N$	coefficient in Gutenberg-Richter relation	13	*Gutenburg and Richter*, 1954
b_N	coefficient in Gutenberg-Richter relation, global average $b_N = 0.9$	13	*Gutenburg and Richter*, 1954;
M_{wmax} M_{wmin}	upper and lower bounds of earthquake moment magnitudes in specified area and time	13	*Malamud et al.*, 2004
$\dot{N}_{CE}$	Earthquake recurence rate	13	*Gutenburg and Richter*, 1954
$\Delta\dot{V}$	net crustal volume addition rate	13	
A_E	equivalent normalized 1°lat.×1°long. area at the equator	14	*Malamud et al.*, 2004
$\dot{h}$	net crustal thickening rate	14	
I_4	number of earthquakes with M ≥ 4 in cosine(latitude)-normalized 1°lat.×1°long. areas per year	14	*Kossobokov et al.*,2000; *Malamud et al.*, 2004
$f(M_w)$	volume contributing fraction function: the volumes of landslides with magnitudes between M_w and $M_w + \delta M_w$ divided by the total uplift volume	16	
δM_w	the size of each magnitude bin	16	

where $\bar{V}_U$ is the dip angle-averaged uplift volume and Θ is the dip angle average term, normalizing the uplift volume over a range of dip angles. Values, standard errors, and sources for all the parameters are reported in Table 2.

We substitute the empirically derived scaling factors for relationships between rupture area and surface displacement and earthquake magnitudes for reverse fault earthquakes [*Wells and Coppersmith*, 1994] into equation (8). We consider values for the dip angle θ in the range of 20°–40°, a geologically reasonable range for the majority of orogenic thrust faults [e.g., *Abers*, 2009; *Shen et al.*, 2009], and obtain the dip angle-averaged uplift volume in terms of magnitude:

$$\log \bar{V}_U = 1.06(\pm 0.22) M_w - 8.40(\pm 1.44) \quad (9)$$

The relation describing the "destructive" coseismic landslide volume as a function of M_w (equation (2)) has a different slope from this relationship, which describes the "constructive" uplift volume as a function of M_w. At low M_w, uplift volume is greater than landslide volume for a given M_w, but at the highest M_w, landslide volume is greater. The relations cross at a value of M_w that defines a threshold, beyond which the volume of seismically induced landslides outweighs volume addition associated with coseismic deformation on the fault. Taking the mean values from the parameterization of each relation, this threshold between earthquakes that have a net positive versus net destructive volume balance would be $M_w \approx 8.0$ (Figure 4a). However, it is important to emphasize that there are very large uncertainties in this analysis given the poor constraints on key parameters, with the largest uncertainty introduced in the fault geometry and scaling parameters used in equation (8), as demonstrated by sensitivity analysis (see Table S4 and Figure S7 in supporting information for details).

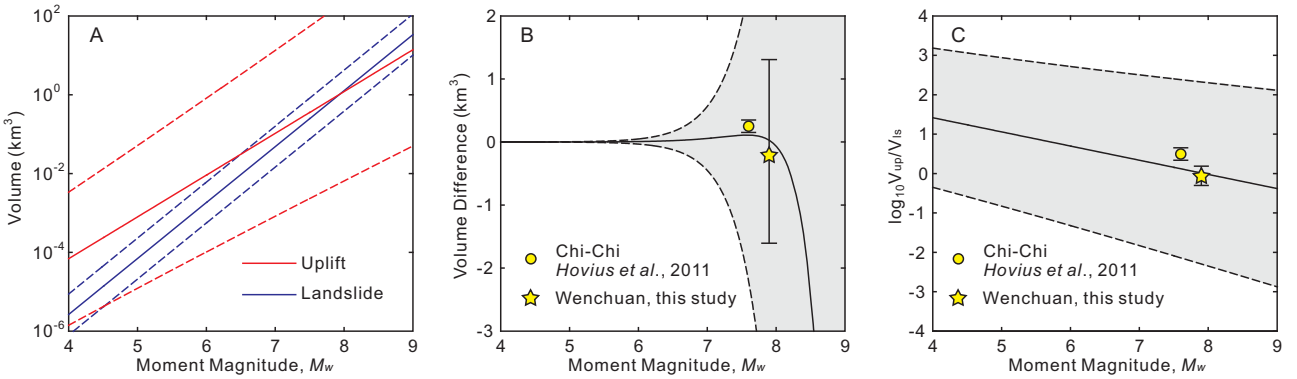

Figure 4. Dependence of volume balance for individual earthquakes with given magnitudes and all earthquakes with varying magnitudes on earthquake moment magnitude M_w. (a) Volume addition due to coseismic rock uplift (red) and volume reduction due to landsliding (blue) for individual earthquakes as a function of M_w. The means of the two terms match at $M_w \approx 8.0$. The blue solid line indicates the least-square best fit straight line to the reported earthquake-triggered landslide inventories, adopted from *Malamud et al.* [2004]. The blue dashed lines represent ± 1 standard deviations with respect to the best fit. The red solid line indicates the theoretical uplift volume estimated from this study, and the red dashed lines show ± 1 standard deviations determined from error propagations of all parameters in equation (8). (b) The difference between volume addition and volume reduction in terms of M_w. (c) The dependency of the ratio of volume addition and volume reduction in logarithmic space. The two events for which volume budgets have been constrained, the Chi-Chi and Wenchuan earthquakes, both fall within the predicted ranges in Figures 4b and 4c. The solid lines in Figures 4b and 4c represent the derived volume difference from this study, and the dashed lines and gray areas show ± 1 standard deviations from error propagation.

The coseismic volume budget can then be determined as the difference of the "constructive" (equation (9)) and "destructive" (equation (2)) terms, as

$$\Delta V = \bar{V}_U - V_L \tag{10}$$

$$\Delta \log V = \log \bar{V}_U - \log V_L \tag{11}$$

Note that equation (11) can be rewritten as the ratio of the two volumes:

$$\Delta \log V = \log \frac{\bar{V}_U}{V_L} \tag{12}$$

Uncertainties on these values (as shown by the dashed line-bounded ranges in Figures 4b and 4c) are propagated via integrated nonlinear error propagation, taking into account uncertainties in the parameter values used (see Table 2). Our result for the Wenchuan earthquake falls within the range predicted by equation (12) (Figures 4b and 4c). The only other documented assessment of earthquake volume balance is from *Hovius et al.* [2011], who estimated the net effect on surface topography for the M_w 7.6 Chi-Chi earthquake in Taiwan using hydrologic and geodetic data. Their study used the sediment load from the epicentral Choshui catchment to calculate landslide material export and indicated that over 30% of the added mass by the earthquake has been removed. Assuming equal density for uplifted rock and eroded sediment, this value for the Chi-Chi earthquake also falls within the range of volume change predicted by our model (Figures 4b and 4c).

We emphasize that this scaling relation-based, first-order volume budget has many large uncertainties, and that the propagation of these uncertainties means that, at present, it is difficult to confidently define the net volume balance of earthquakes. Many of the scaling parameters, particularly those associated with coseismic uplift, require further quantification before this problem can be fully understood. Moreover, the geometry of real fault systems is considerably more complex than our simplified model, which considers only displacement on a single reverse fault. In addition, in our analysis we consider deformation in an ideal, elastic half-space [*Okada*, 1992], which does not include the effects of viscoelastic response that can contribute importantly to mountain building and may also scale with earthquake magnitude [e.g., *King et al.*, 1988]. Future work might consider a viscous half-space framework. We also assume no spatial variation in landslide susceptibility, which is controlled by a number of factors (e.g., lithology, topography, climatic conditions, and epicentral depth). These parameters are beyond the scope of our study, but will require further consideration to develop a complete picture of the earthquake volume balance problem. Nonetheless, given the reasonable accordance with data from the two presently available earthquake events, we suggest

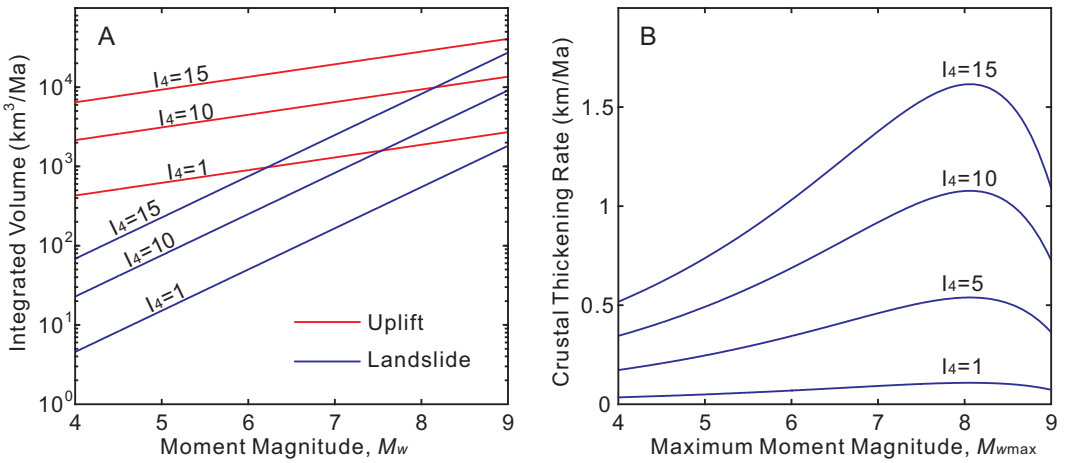

Figure 5. Dependence of coseismic volume balance for all earthquakes with varying magnitudes on earthquake moment magnitude M_w. (a) Integrated volume surplus and deficit for earthquakes with varying magnitudes versus M_w. (b) Integrated crustal thickening rate during coseismic deformation as a function of I_4 and M_{wmax}.

that the concept developed here provides a meaningful general framework for considering the coseismic contribution to the volume balance of earthquakes, which with further refinement can be used to probe the role of seismicity in the production of surface topography and associated crustal thickening.

It is also important to note that the apparent volume balance of a given earthquake as developed here also does not predict the total topographic effects of a single event. For example, in the Wenchuan case, the zone of surface uplift ($<$15 km from the surface rupture assuming this zone is defined by focal depth $\times$ tan(θ), and using focal depth d $\sim$ 14–18 km and dip angle $\theta \sim$ 40–90°) is much smaller that the region of observed coseismic landslides (which range up to $\sim$100 km from the surface rupture). Moreover, small spatial-scale topographic features such as observable fault scarps may remain evident despite regional-scale volume loss via landslides. The difference in the spatial scale of rock uplift versus landslide removal will play a role in mass redistribution within mountain ranges, and may have important consequent effects on tectonic processes [*Egholm et al*., 2013; *Parker et al*., 2011; *King et al*., 1988], but the overall volume balance of earthquakes in terms of topographic evolution only makes sense when integrated over large areas and over long periods of time (e.g., the time scale of seismic cycles on major faults).

5.3. Integrated Volume Balance for Multiple Earthquake Events

The seismic contribution to mountain building and crustal thickening is not controlled by one single earthquake, but is the accumulated result of multiple seismic cycles [*Avouac*, 2007]. This means that understanding the seismic role in mountain building is further complicated by the varying recurrence rates of earthquakes with dissimilar magnitudes in different tectonic settings. To account for these variable seismic parameters, we incorporate the Gutenberg-Richter frequency-magnitude relation and a seismic-intensity factor to estimate the cumulative effect of earthquakes on coseismic crustal volume balance and the coseismic crustal thickening that contributes to building mountainous topography.

The Gutenberg-Richter frequency-M_w relation [*Gutenburg and Richter*, 1954] describes the frequency of earthquakes in a specified region as a function of earthquake moment magnitude M_w, and thus allows the integration of volume budget effects from earthquakes of varying magnitudes. Using the Gutenberg-Richter frequency-M_w relation, we can calculate the total coseismic uplift and landslide volumes from all earthquake events (Figure 5a; see details in supporting information). The rate of net coseismic volume addition is then derived as the difference of the surplus term and the deficit term:

$$\Delta\dot{V} = \frac{\dot{a}_N b_N \Theta}{b_A + b_D - b_N} 10^{(a_A + a_D) + (b_A + b_D - b_N) M_{wmax}} - \frac{\dot{a}_N b_N}{b_L - b_N} 10^{a_L + (b_L - b_N) M_{wmax}} \tag{13}$$

where a_A, b_A, a_D, and b_D are parameters in the fault rupture geometry parameters-M_w relations, $\dot{a}_N$ and b_N are parameters in the Gutenberg-Richter relation, a_L and b_L are parameters in the landslide volume-M_w

relation, Θ is the dip angle averaging term, and $M_{w\max}$ is the maximum observed magnitude for all earthquakes within the study area.

Introducing a regional seismic-intensity factor, I_M, makes it possible to consider the spatial variation of the frequency of mountain-building earthquakes. This factor expresses the regional seismic intensity as the number of earthquakes with magnitudes greater than or equal to M_w in specified region (defined as a 1° longitude × 1° latitude area) per year [*Malamud et al*., 2004]. Although a complete data set recording all earthquakes is not available, *Kossobokov et al*. [2000] has compiled a global map of I_4, showing the spatial variation of occurrence rates for earthquakes with magnitude greater than or equal to $M_w = 4$. The global data set of the seismic-intensity factor I_4 thus allows calculation of earthquake frequency in different settings. Note that magnitude 4 is also the approximate cutoff magnitude of earthquakes observed to generate landslides [*Keefer*, 2002]. Combining the seismic-intensity factor, the global I_4 data set, and the Gutenberg-Richter relation-based cumulative earthquake volume budget model (equation (13)), we convert volume change to a rate of crustal thickening by assuming that the additional material is spread uniformly over the 1° × 1° area of defined seismic intensity from the *Kossobokov et al*. [2000] compilation. We thus obtain a generalized analytical expression for estimating the rate of seismically induced crustal thickening in terms of the observed maximum earthquake moment magnitude $M_{w\max}$ in the study area, and the regional seismic-intensity factor I_4 (see supporting information for derivation):

$$\dot{h} = \frac{1}{A_E}\left(\frac{b_N\Theta}{b_A+b_D-b_N}10^{(a_A+a_D)+(b_A+b_D-b_N)M_{w\max}} - \frac{b_N}{b_L-b_N}10^{a_L+(b_L-b_N)M_{w\max}}\right)I_4 10^{4b_N} \tag{14}$$

where $\dot{h}$ is the crustal thickening rate (km Ma^{-1}) during coseismic deformation and A_E is the equivalent normalized 1° × 1° area at the equator (~111 × 111 km^2). The numerical results can be derived by substituting all parameters (Table 2) into equation (14), giving:

$$\dot{h} = (6.70 \times 10^{0.16M_{w\max}-3} - 3.07 \times 10^{0.52M_{w\max}-6})I_4 \tag{15}$$

The dependence of crustal thickening rate on $M_{w\max}$ and I_4 is shown in Figure 5b. Referring to the compiled global spatial distribution of I_4 and $M_{w\max}$ in *Kossobokov et al*. [2000], we may derive first-order coseismic crustal thickening rates for specific regions using equation (15). Then this generalized coseismic mountain building and crustal thickening model can be compared to observed orogenic uplift and exhumation rates. The Himalaya, a typical continental-continental collision zone characterized by thrust-fault earthquakes, provides an example. In this case, $I_4 \approx$ 1–5 earthquakes yr^{-1} and $M_{w\max} \approx 9$ on the global I_4 and $M_{w\max}$ maps [*Kossobokov et al*., 2000], and the resulting modeled coseismic crustal thickening rates are around 0.1–0.5 km Ma^{-1}. Though this is potentially geologically reasonable, rigorous validation and refinement of this generalized model will require further careful assessment. It is also important to note that our model is based on empirical parameterizations that are specific to thrust fault settings. Nonetheless, considering the large uncertainties on geodynamic parameters at orogenic scales, our model provides a first-order estimation of coseismic cumulative crustal volume change, and most importantly presents a new conceptual approach for considering this problem quantitatively.

5.4. Relative Overall Contributions to Coseismic Mountain Building From Earthquakes of Varying Magnitude

We can estimate the contributions to the total volume of uplifted rock as a result of coseismic deformation from earthquakes with specified magnitudes, and define a volume contributing fraction function $f(M_w)$:

$$f(M_w) = \frac{\Delta\dot{V}(M_w+\delta M_w) - \Delta\dot{V}(M_w)}{\Delta\dot{V}_{total}} \tag{16}$$

where $\Delta\dot{V}_{total}$ is the total uplift volume across the range of all magnitudes (determined as the difference between the maximum net uplift volume and the net uplift volume at $M_w = 4$) and δM is the size of each magnitude bin (set here to be $\delta M_w = 0.1$). For $4 \le M_w \le 9$, the contributions to the total rock uplift volume

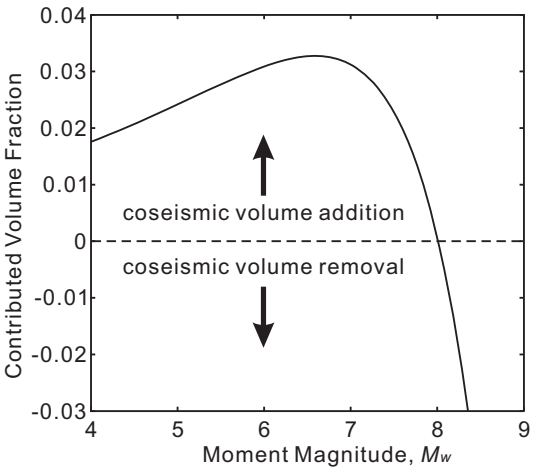

Figure 6. Contributions to the total coseismic orogenic volume from earthquakes of varying magnitudes. The total coseismic orogenic volume is calculated as the total uplift volume in the range of all magnitudes. The contributed volume fraction refers to the contribution to the total coseismic uplift volume from earthquakes with magnitudes in each bin (set here to be $\delta M_w = 0.1$), as indicated in equation (16).

from different earthquakes are shown in Figure 6. The distribution of added fractions suggests that moderate to large earthquakes ($6 \leq M_w \leq 7$) add most to the total orogenic volume through coseismic deformation, while the very largest earthquakes may be net destructive because of the much more significant landslide volume reduction effects at larger magnitudes.

6. Conclusion

We mapped the Wenchuan earthquake-triggered landslides by combining automated extraction and manual segregation of landslide clusters. The total calculated landslide volume is $\sim 2.8 + 0.9/-0.7$ km^3. This revises the initial estimate of *Parker et al*. [2011], but confirms that coseismic volume removal may significantly counteract seismically induced orogenic growth. The uncertainty in our estimated volume of Wenchuan-triggered landslides remains significant largely because of weak constraints on the parameters in the area-volume scaling relationships used in the calculation. Better understanding of the sources of parametric uncertainties in this scaling relation, or other direct approaches to determine volumes, will be required to reduce such uncertainties. To consider whether the observations from Wenchuan are generalizable, we develop a model of thrust fault associated uplift that allows us to evaluate the volume balance for earthquakes with specified magnitudes. We find that there may be a threshold earthquake magnitude above which volume wasting from coseismic landsliding exceeds earthquake-triggered volume growth. The very large uncertainties in the parameterizations used in our analysis hamper clear definition of the magnitude of this threshold, with the greatest uncertainty coming from the parameterization of coseismic uplift but uncertainty in global landslide volume-M_w relation also significant. Future work building on this conceptual framework might reduce these uncertainties. By incorporating the Gutenburg-Richter relation and the seismic-intensity factor I_4, we estimate the cumulative effect for all earthquakes in different regions. Assuming efficient erosion and fluvial export, and using the mean values of fault geometry and coseismic landslide volume from our parameterization, the net crustal thickening rates associated with coseismic deformation in typical continental-continental collision zones (e.g., the Himalaya) would be on the order of $\sim$0.1–0.5 km Ma^{-1}. Based on our analysis and the global earthquake inventory, the earthquakes that contribute most to crustal thickening and mountain building are probably medium to large events with magnitudes of 6-7, although future work to reduce uncertainties is clearly warranted. Such work might make it possible to better quantify the coseismic contribution to deformation, and to then be able to relate this to other sources of information such as geodetic observations.

Acknowledgments

This research was supported by the U.S. National Science Foundation (NSF-EAR/GLD grant 1053504 to A.J.W.), the Chinese Academy of Sciences (YIS fellowship grant 2011Y2ZA04 to A.J.W.), the Royal Society (Research Grant RG110569 to R.G.H.), and benefited from imagery provided by the Polar Geospatial Data Center and DigitalGlobe. We thank Niels Hovius for helpful discussions, Siobhan Whadcoat for providing the Wenchuan landslide field measurements data set, and two anonymous reviewers for their insightful comments, which significantly improved the manuscript.

References

Abers, G. A. (2009), Slip on shallow-dipping normal faults, *Geology*, *37*(8), 767–768, doi:10.1130/focus082009.1.

Avouac, J. P. (2007), 6.09—Dynamic processes in extensional and compressional settings—Mountain building: From earthquakes to geological deformation, in *Treatise on Geophysics*, edited by S. Gerald, pp. 377–439, Elsevier, Amsterdam, doi:10.1016/B978-044452748-6.00112-7.

Borghuis, A. M., K. Chang, and H. Y. Lee (2007), Comparison between automated and manual mapping of typhoon-triggered landslides from SPOT-5 imagery, *Int. J. Remote Sens.*, *28*(7–8), 1843–1856, doi:10.1080/01431160600935638.

Burchfiel, B. C., Z. L. Chen, Y. Liu, and L. H. Royden (1995), Tectonics of the Longmen Shan and adjacent regions, central China, *Int. Geol. Rev.*, *37*(8), 661–735, doi:10.1080/00206819509465424.

Cohen, S. C. (1996), Convenient formulas for determining dip-slip fault parameters from geophysical observables, *Bull. Seismol. Soc. Am.*, *86*(5), 1642–1644.

Dadson, S. J., et al. (2004), Earthquake-triggered increase in sediment delivery from an active mountain belt, *Geology*, *32*(8), 733–736, doi:10.1130/G20639.1.

Dai, F. C., C. Xu, X. Yao, L. Xu, X. B. Tu, and Q. M. Gong (2011), Spatial distribution of landslides triggered by the 2008 Ms 8.0 Wenchuan earthquake, China, *J. Asian Earth Sci.*, *40*(4), 883–895, doi:10.1016/j.jseaes.2010.04.010.

de Michele, M., D. Raucoules, J. de Sigoyer, M. Pubellier, and N. Chamot-Rooke (2010), Three-dimensional surface displacement of the 2008 May 12 Sichuan earthquake (China) derived from synthetic aperture radar: Evidence for rupture on a blind thrust, *Geophys. J. Int.*, *183*(3), 1097–1103, doi:10.1111/j.1365-246X.2010.04807.x.

Densmore, A. L., M. A. Ellis, Y. Li, R. J. Zhou, G. S. Hancock, and N. Richardson (2007), Active tectonics of the Beichuan and Pengguan faults at the eastern margin of the Tibetan Plateau, *Tectonics*, *26*, TC4005, doi:10.1029/2006TC001987.

Densmore, A. L., R. N. Parker, N. J. Rosser, M. de Michele, Y. Li, R. Q. Huang, S. Whadcoat, and D. N. Petley (2012), Reply to 'Isostasy can't be ignored', *Nat. Geosci.*, *5*(2), 83–84, doi:10.1038/ngeo1385.

Egholm, D. L., M. F. Knudsen, and M. Sandiford (2013), Lifespan of mountain ranges scaled by feedbacks between landsliding and erosion by rivers, *Nature*, *498*(7455), 475–478, doi:10.1038/nature12218.

Fu, Z., C. B. Hu, H. M. Zhang, Y. G. Cai, and Y. J. Zhou (2011), The possibility of inferring rupture depths of fault earthquakes from zero-strain points of coseismic surface deformation, *Seismol. Res. Lett.*, *82*(1), 89–96, doi:10.1785/gssrl.82.1.89.

Godard, V., R. Pik, J. Lave, R. Cattin, B. Tibari, J. de Sigoyer, M. Pubellier, and J. Zhu (2009), Late Cenozoic evolution of the central Longmen Shan, eastern Tibet: Insight from (U-Th)/He thermochronometry, *Tectonics*, *28*, TC5009, doi:10.1029/2008TC002407.

Gutenberg, B., and C. F. Richter (1954), *Seismicity of the Earth and Associated Phenomenon*, 2nd ed., Princeton Univ. Press, Princeton, N. J.

Guzzetti, F., F. Ardizzone, M. Cardinali, M. Rossi, and D. Valigi (2009), Landslide volumes and landslide mobilization rates in Umbria, central Italy, *Earth Planet. Sci. Lett.*, *279*(3–4), 222–229, doi:10.1016/j.epsl.2009.01.005.

Hovius, N., P. Meunier, C. W. Lin, H. Chen, Y. G. Chen, S. Dadson, M. J. Horng, and M. Lines (2011), Prolonged seismically induced erosion and the volume balance of a large earthquake, *Earth Planet. Sci. Lett.*, *304*(3–4), 347–355, doi:10.1016/j.epsl.2011.02.005.

Keefer, D. K. (1994), The importance of earthquake-induced landslides to long-term slope erosion and slope-failure hazards in seismically active regions, *Geomorphology*, *10*(1–4), 265–284, doi:10.1016/0169-555X(94)90021-3.

Keefer, D. K. (2002), Investigating landslides caused by earthquakes—A historical review, *Surv. Geophys.*, *23*(6), 473–510, doi:10.1023/A:1021274710840.

King, G. C. P., R. S. Stein, and J. B. Rundle (1988), The growth of geological structures by repeated earthquakes: 1. Conceptual framework, *J. Geophys. Res.*, *93*(B11), 13,307–13,318, doi:10.1029/JB093iB11p13307.

Korup, O., A. L. Densmore, and F. Schlunegger (2010), The role of landslides in mountain range evolution, *Geomorphology*, *120*(1–2), 77–90, doi:10.1016/j.geomorph.2009.09.017.

Kossobokov, V. G., V. I. Keilis-Borok, D. L. Turcotte, and B. D. Malamud (2000), Implications of a statistical physics approach for earthquake hazard assessment and forecasting, *Pure Appl. Geophys.*, *157*(11–12), 2323–2349, doi:10.1007/PL00001086.

Larsen, I. J., D. R. Montgomery, and O. Korup (2010), Landslide erosion controlled by hillslope material, *Nat. Geosci.*, *3*(4), 247–251, doi:10.1038/ngeo776.

Liu-Zeng, J., et al. (2009), Co-seismic ruptures of the 12 May 2008, Ms 8.0 Wenchuan earthquake, Sichuan: East-west crustal shortening on oblique, parallel thrusts along the eastern edge of Tibet, *Earth Planet. Sci. Lett.*, *286*(3–4), 355–370, doi:10.1016/j.epsl.2009.07.017.

Malamud, B. D., D. L. Turcotte, F. Guzzetti, and P. Reichenbach (2004), Landslides, earthquakes, and erosion, *Earth Planet. Sci. Lett.*, *229*(1–2), 45–59, doi:10.1016/j.epsl.2004.10.018.

Meunier, P., N. Hovius, and A. J. Haines (2007), Regional patterns of earthquake-triggered landslides and their relation to ground motion, *Geophys. Res. Lett.*, *34*, L20408, doi:10.1029/2007GL031337.

Molnar, P. (2012), Isostasy can't be ignored, *Nat. Geosci.*, *5*(2), 83–83, doi:10.1038/ngeo1383.

Okada, Y. (1985), Surface deformation due to shear and tensile faults in a half-space, *Bull. Seismol. Soc. Am.*, *75*(4), 1135–1154.

Okada, Y. (1992), Internal deformation due to shear and tensile faults in a half-space, *Bull. Seismol. Soc. Am.*, *82*(2), 1018–1040.

Ouimet, W. B., K. X. Whipple, and D. E. Granger (2009), Beyond threshold hillslopes: Channel adjustment to base-level fall in tectonically active mountain ranges, *Geology*, *37*(7), 579–582, doi:10.1130/G30013A.1.

Parker, R. N., A. L. Densmore, N. J. Rosser, M. de Michele, Y. Li, R. Q. Huang, S. Whadcoat, and D. N. Petley (2011), Mass wasting triggered by the 2008 Wenchuan earthquake is greater than orogenic growth, *Nat. Geosci.*, *4*(7), 449–452, doi:10.1038/ngeo1154.

Ran, Y. K., L. C. Chen, J. Chen, H. Wang, G. H. Chen, J. H. Yin, X. A. Shi, C. X. Li, and X. W. Xu (2010), Paleoseismic evidence and repeat time of large earthquakes at three sites along the Longmen Shan fault zone, *Tectonophysics*, *491*(1–4), 141–153, doi:10.1016/j.tecto.2010.01.009.

Ren, Z. K., Z. Q. Zhang, J. H. Yin, F. C. Dai, and H. P. Zhang (2014), Morphogenic uncertainties of the 2008 Wenchuan earthquake: Generating or reducing?, *J. Earth Sci.*, in press.

Shen, Z. K., J. B. Sun, P. Z. Zhang, Y. G. Wan, M. Wang, R. Burgmann, Y. H. Zeng, W. J. Gan, H. Liao, and Q. L. Wang (2009), Slip maxima at fault junctions and rupturing of barriers during the 2008 Wenchuan earthquake, *Nat. Geosci.*, *2*(10), 718–724, doi:10.1038/ngeo636.

Wells, D. L., and K. J. Coppersmith (1994), New empirical relationships among magnitude, rupture length, rupture width, rupture area, and surface displacement, *Bull. Seismol. Soc. Am.*, *84*(4), 974–1002.

West, A. J., C. W. Lin, T. C. Lin, R. G. Hilton, S. H. Liu, C. T. Chang, K. C. Lin, A. Galy, R. B. Sparkes, and N. Hovius (2011), Mobilization and transport of coarse woody debris to the oceans triggered by an extreme tropical storm, *Limnol. Oceanogr.*, *56*(1), 77–85, doi:10.4319/lo.2011.56.1.0077.

Xu, X., X. Wen, G. Yu, G. Chen, Y. Klinger, J. Hubbard, and J. Shaw (2009), Coseismic reverse- and oblique-slip surface faulting generated by the 2008 M_w 7.9 Wenchuan earthquake, China, *Geology*, *37*(6), 515–518, doi:10.1130/g25462a.1.